Double-pulse laser ablation sampling: Enhancement of analyte emission by a second laser pulse at 213 nm

Bruno Yue Cai[1, 2], Xianglei Mao[1], Huaming Hou[1, 3], Vassilia Zorba[1], Richard E. Russo[1] and Nai-Ho Cheung[2, *]

[1] Laser Technologies Group, Lawrence Berkeley National Laboratory, Berkeley, CA, USA.

[2] Department of Physics, Hong Kong Baptist University, Kowloon Tong, Hong Kong, China.

[3] Ocean University of China, Qingdao, China

* Corresponding author. Email address: nhcheung@hkbu.edu.hk (N.-H. Cheung).

Abstract

For the purpose of devising methods for minimally destructive multi-element analysis, we compare the performance of a 266 nm – 213 nm double-pulse scheme against that of the single 266 nm pulse scheme. The first laser pulse at 266 nm ablates a mica sample. Ten ns later, the second pulse at 213 nm and 64 mJ cm^{-2} orthogonally intercepts the gas plume to enhance the analyte signal. Emissions from aluminum, silicon, magnesium and sodium are simultaneously observed. At low 266 nm laser fluence when only sub-ng of sample mass is removed, the signal enhancement by the 213 nm pulse is especially apparent. The minimum detectable amount of aluminum is about 24 fmol; it will be a hundred times higher if the sample is analyzed by the 266 nm pulse alone. The minimum detectable mass for the other analytes is also reduced by about two orders of magnitude when the second pulse at 213 nm is introduced. The spectral and temporal properties of the enhanced signal are consistent with the mechanism of ultra-violet laser excited atomic fluorescence of dense plumes.

Keywords

double laser pulse scheme, plume-LEAF, pulsed laser ablation sampling, 213 nm, minimally destructive multi element analysis

1. Introduction

While laser-induced breakdown spectroscopy (LIBS) has proven to be a versatile analysis technique, its sensitivity can be further enhanced by a two-pulse approach [1,2]. The enhanced sensitivity is particularly useful when the mass removed has to be minimized, as in nondestructive analysis [3] or in high spatial resolution mapping [4].

We previously demonstrated two-pulse LIBS analysis of crystalline silicon at better than 2 μm lateral resolution [5]. The first laser pulse of 500 fs at 343 nm ablated the sample to create a plume of short luminous lifetime. A second laser pulse of 6 ns duration at 355 nm orthogonally intercepted the plume to enhance and sustain the signal. The analyte spectral intensity was amplified by two orders of magnitude while the minimum detectable mass was reduced 50-fold.

In another recent study, we performed two-pulse forensic analysis of inks and pigments on questioned documents [6]. For this application, visible damage of the legal specimen was not allowed. Here again, the first laser pulse removed only sub-ng of the sample. The plume produced was too cold to be emissive. The analyte signal was induced by a second laser pulse of 10 ns width at 193 nm that intercepted the plume perpendicularly. Minimum detectable mass in the atto-mole range was achieved.

The signal enhancement mechanisms in the two studies are very different. In the silicon case, the second laser pulse at fluences of tens of J cm^{-2} reheated and ionized the plume to generate spectral emission that lasted hundreds or even thousands of ns and outlived the initial continuum background. This situation is typical in two-pulse LIBS configurations [1]. In the questioned document case, the fluence of the second laser pulse was only 42 mJ cm^{-2}, there was minimal background

and the enhanced emissions lasted no more than 100 ns, all suggestive of 193-nm laser excited atomic fluorescence (LEAF) of dense plumes.

Various applications of the plume-LEAF scheme at 193 nm excitation have been reported [7 - 12]. Plausible models of the physical mechanism were also discussed [8,13]. It was conjectured that two factors are essential for the signal enhancement, near-solid plume density and high photon energy. Accordingly, plume interception at other ultra-violet wavelengths should be equally effective. For example, the fifth harmonic of the Nd:YAG laser at 213 nm would be an interesting alternative, not only because of the high photon energy, but also because of the ease of operation when compared to the 193 nm ArF excimer laser.

In this work, we investigate the effectiveness of using a 213 nm laser pulse as the signal enhancing second pulse. We quantify the improvement by estimating the minimum detectable mass with and without the second pulse, and draw observations that help to elucidate the signal enhancement mechanisms.

2. Experimental

Mica samples were chosen as test samples because they were atomically flat and contained major and minor elements of interest [14]. Their surface properties and chemical compositions were consistent from batch to batch. The major elements were Si and Al; the minor elements were Mg and Na [14]. These analytes have strong emission lines that are spaced spectrally without interferences.

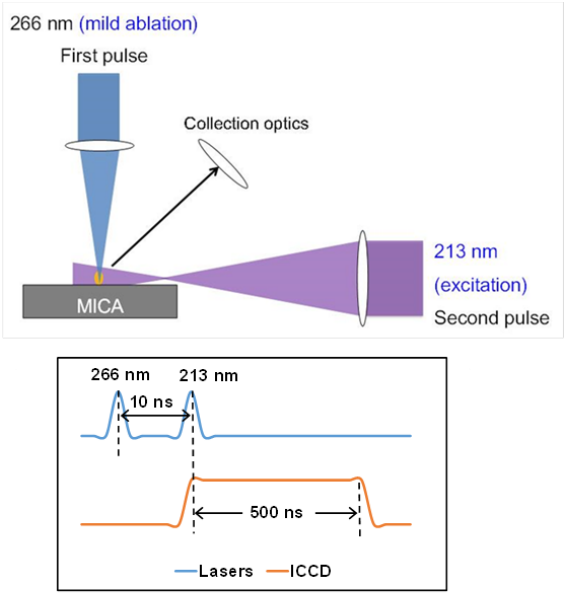

Fig. 1. Experimental schematics for doing 266-213 two-pulse laser sampling of mica samples.

The experimental setup was similar to the one reported previously [5]. It is shown schematically in Fig. 1. Briefly, a Nd:YAG laser pulse (New Wave, fourth harmonic at 266 nm, 10 Hz, 6 ns) was delivered normally through a 100 mm f.l. lens onto the mica sample which was either stationary or translated. The laser fluence ranged from 330 mJ cm^{-2} for gentle ablation to more than 800 mJ cm^{-2} for LIBS analysis. The corresponding crater diameter ranged from 16 μm to 150 μm. After a delay Δt, the ablated plume was intercepted transversely by a second Nd:YAG laser pulse (Quantel, fifth harmonic at 213 nm, 10 Hz, 6 ns). The 213 nm beam was focused through a 150 mm focal length lens to a waist of about 40 μm in diameter and

10 mm in front of the plume. It diverged to a 2 mm diameter spot at the plume. The inter-pulse delay Δt was set at 10 ns so that the second pulse could interact with the expanding plume at its maximum density. At such short interpulse delay, the plume was extended only tens of μm above the target so the 213 nm beam had to be close to the target surface. The energy of the second pulse was therefore capped at 2 mJ to avoid ablating the sample. The corresponding fluence was about 64 mJ cm^{-2} at the plume.

The spectral emissions were collected along a direction 45° from the surface normal of the mica sample and focused through a 50 mm focal length lens onto an optical fiber bundle. The other end of the fiber bundle was connected to a 60 μm-wide slit entrance of a spectrometer/ICCD camera system (Acton SP150/Princeton Instruments PI-MAX). The gain of the ICCD was set to 250. The instrumental spectral resolution was about 0.3 nm, which was preserved in all off-line spectral smoothing. The ICCD was gated on ten ns after the 266 nm pulse, and stayed on for 500 ns.

The morphology of the ablated crater was characterized by a white light interferometer (Zygo Multiview 6K) that featured an *x*-*y* resolution of 710 nm (with 20× NewView TM6000 objective) and a *z*-resolution of 0.1 nm.

Further experimental details specific to particular data sets are given either in the relevant sections or in the figure captions.

3. Results and Discussion

The spectra produced by a low fluence 266 nm pulse of 330 mJ cm^{-2} are shown in the lower panel of Fig. 2. The spectrum produced by the 266 nm pulse alone is shown in red. That produced by the 266 nm-213 nm two-pulse scheme is shown in blue. Each spectrum is the sum of 100 sampling events. The two traces are offset vertically for clarity, with the leading and trailing pixels zeroed to indicate the baseline. As can be seen, the 266 nm single-pulse configuration produced no analyte emission while the 266 nm -213 nm scheme produced strong signals.

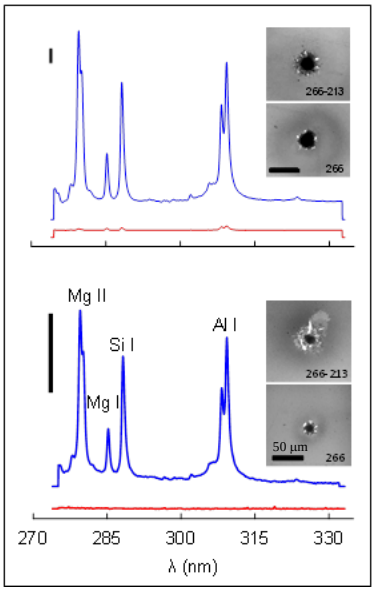

Fig. 2. Spectra produced by 266 nm laser sampling of mica at two laser fluences, 330 mJ cm^{-2} (bottom panel) and 380 mJ cm^{-2} (top panel). In each case, two spectra are shown, one generated by the 266 nm laser pulse alone (red trace) and one produced by the 266 nm – 213 nm scheme (blue trace). Each trace is the sum of 100 sampling events. The *y* scale of the bottom panel is amplified 5.5× relative to the top panel. The intensity scale bar represents 40,000 CCD counts in each panel. The Mg II 279.6 and 280.3 nm doublet, the Mg I 285.2 nm and Si I 288.2 nm lines, and the Al I 308.2 and 309.3 nm doublet are shown. Inset shows the corresponding craters after 100 sampling events. Scale bar is 50 µm.

We should point out that without the 266 nm first pulse, the 213 nm pulse produced neither ablation nor analyte signal. However, with the 266 nm ablative first

pulse, the 213 nm second pulse removed additional sample material despite the orthogonal arrangement. This is evident from the crater images shown in the inset of Fig. 2. We estimated the mass removed based on the crater volume and the mica density. With 266 nm pulse alone, 0.34 ng was removed after one hundred shots. With 213 nm pulse added, 0.60 ng was removed. The extra mass removed might be explained by the fact that the 213 nm beam glanced and further vaporized part of the hot and presumably molten sample surface (see Fig. 1). Another possibility is that the 213 nm beam enhanced the plume-target interactions.

When the fluence of the first pulse was increased to 380 mJ cm^{-2}, the analyte signal became visible in the 266 nm laser-induced spectrum. This is depicted by the red trace in the top panel of Fig. 2. Notice that the vertical scale is shrunk 5.5× relative to that of the bottom panel for plotting convenience. The crater was bigger now, as shown in the corresponding inset. The mass removed was 1.8 ng after one hundred shots. With the 213 nm laser interception, the signals were orders of magnitude enhanced (blue trace) and the mass removed was 3.0 ng.

To quantify the enhancement of the 213 nm laser interception, we repeated the ablation sampling at a few more 266 nm laser fluences. We plotted the signal-to-noise ratio (SNR, in unit of thousands) of the aluminum Al I 308.2 and 309.3 nm doublet against the mica mass Δm removed per 100 shots. The results are shown in Fig. 3 for both 266 nm (red crosses) and 266 nm-213 nm (blue circles) schemes. Signal and noise are defined as follows. For each 100-shot spectrum, the analyte intensity was defined as the average intensity of the aluminum doublet over a 4.6 nm spectral width with the background subtracted; and background was defined as the average intensity of a featureless region from 329.73 nm to 334.33 nm. Signal was defined as the average analyte intensity of five 100-shot spectra. Noise was defined

as the standard deviation of the background intensity among the five sets. As can be seen, at low Δm, the 266 nm-213 nm trend line (blue) is much steeper than the 266 trend line (red line). Correspondingly, the mass limit-of-detection (mLOD) is much lower.

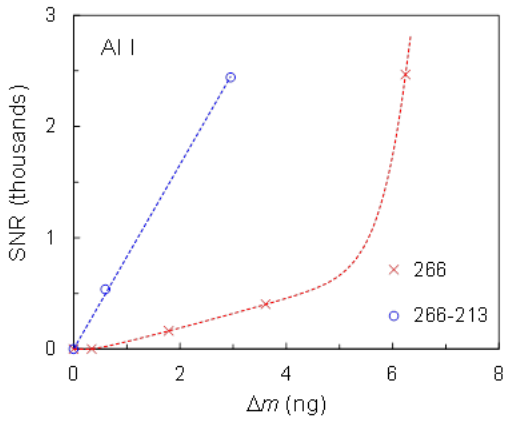

Fig. 3. Plot of 100-shot SNR against the sample mass Δm ablated for the 266 (red crosses) and 266-213 (blue circles) sampling schemes, for the case of Al I 308.2 and 309.3 nm doublet. For the 266 scheme, five laser fluences were used: 0, 330, 380, 410, and 460 mJ cm^{-2}, corresponding to five Δm's. For the 266-213 scheme, three 266 nm laser fluences were used: 0, 330, and 380 mJ cm^{-2}. The data points were curve-fitted with the best trend lines.

We estimated the mLOD for the detection of aluminum by interpolating Δm at SNR equals to three and computed the corresponding analyte mass based on the known aluminum content in mica [14]. For the 266 scheme, mLOD is 2.5 nmol. For the 266 nm-213 nm scheme, it is 24 fmol, or 110× more sensitive. The trend in Fig. 3 suggests that the sensitivity of the 266 nm configuration will improve significantly at higher Δm, though at the expense of considerably more sample mass removed.

We generalized the mLOD estimates to other analytes whose spectral lines were visible. They included magnesium, silicon, and sodium. Their SNR versus Δm plots are shown in Fig. 4. The corresponding mLODs are summarized in Table 1. As can be seen from the table, the 213 nm interception reduced the mLOD by about two

orders of magnitude for all analytes except Mg I. The mLOD of Mg I was lowered by only 37×, but it was compensated by the 170× improvement in the detection of its ion.

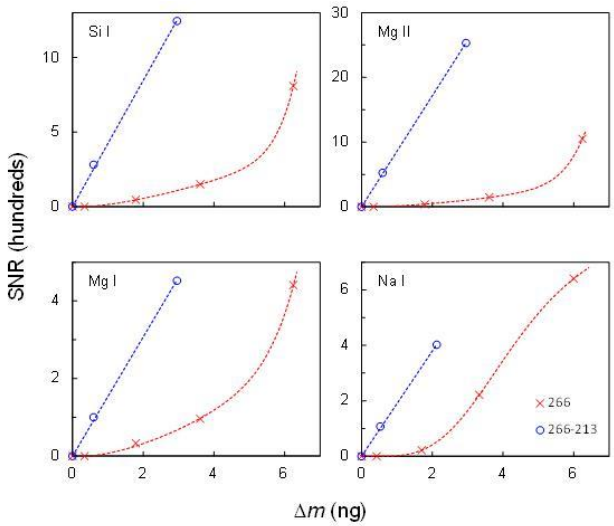

Fig. 4. SNR plotted against the sample mass Δ*m* ablated, for the 266 (red crosses) and 266-213 (blue circles) sampling schemes. Data based on four analyte emissions are shown: Si I 288.2 and Mg I 285.2 nm lines, and Mg II 279.6 and 280.3 and Na I 589.0 and 589.6 nm doublets. Data processing was similar to that of Fig. 3.

Table 1.
Mass LOD based on the various analyte emissions, as measured by the 266 nm and the 266 nm -213 nm schemes.

Analyte emissions	Conc. (%)[a]	mLOD (fmol) 266	266 - 213	Enhancement factor
Mg II 279.6/280.3 nm	0.23	57	0.33	170
Al I 308.2/309.3 nm	17.5	2500	24	110
Si I 288.2 nm	21.3	4300	54	80
Na I 589.0/589.6 nm	0.46	220	3.2	70
Mg I 285.2 nm	0.23	68	1.8	37

[a] Vendor specification [14].

The mechanism of the 213 nm enhancement is briefly considered in the present study. On the one hand, the simultaneous emission by multiple analytes suggests non-selective electron-impact excitation as in LIBS. On the other hand, the prompt signal and low background seems to imply fluorescence. Earlier, we reported similar enhancements by 193 nm ArF laser interception [8,13]. We presented observations that precluded laser-induced breakdown by the ArF pulse. Instead, the observations were more consistent with ArF laser-induced fluorescence of dense plumes [13]. Here, we have similar observations. First, the very weak 213 nm pulse at 64 mJ cm^{-2} could not induce thermal breakdown of the cooling plume. Second, the optical background at the initial time was too dim to be plasma continuum emissions (see Fig. 2). Third, the analyte signal promptly emerged with the 213 nm pulse. No plasma cooling delay was observed. This is shown in Fig. 5 when the various analyte emission intensities are plotted against the ICCD gate delay. Fourth, the signal persistence was too short for typical LIBS signal. Based on Fig. 5, the Al I persistence was measured to be about 15 ns, which is consistent with the 14 and 17 ns radiative lifetime of the doublet [15]. The measured persistence of the other analytes ranged from about 8 ns for Mg II to about 11 ns for Si I, which is consistent with the convolution of the 6 ns width of the 213 nm pulse and the radiative lifetimes of the respective transitions [15]. . The fifth observation further supports fluorescence over plume heating. If this was two-pulse LIBS, we would expect to see stronger signal if the wavelength of the second pulse was longer because it would heat the plasma more efficiently by inverse *Bremsstrahlung* [16,17]. However, as Fig. 6 shows, our observation was the opposite. The signal produced by 266-266 (red) was weaker than the 266-213 case (blue). All in all, the spectral and temporal properties of the

enhanced signal were consistent with the plume-LEAF model [8,13]. More experiments are underway to further elucidate the mechanism.

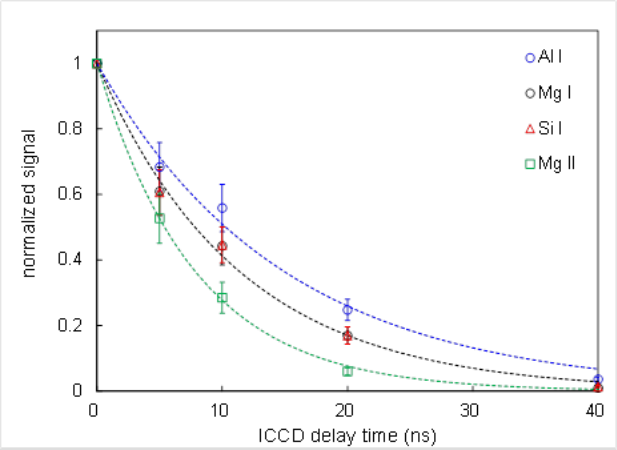

Fig. 5. Signal versus ICCD delay for the four analyte emissions indicated. The first 266 nm pulse was at a fluence of 330 mJ cm^{-2}. Ten ns later, the plume was intercepted by the 213 nm pulse. ICCD gate delay was measured from the second 213 nm pulse; the gate width was 500 ns. Best exponential fits are shown.

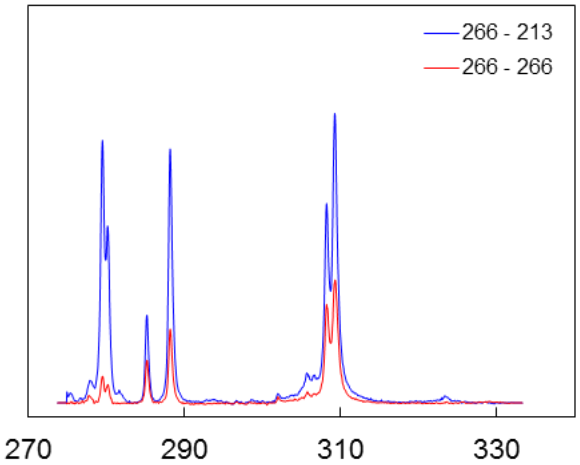

Fig. 6. Spectra produced by laser sampling of mica using two schemes: (1) 266-266 (red trace) and 266-213 (blue trace). The fluence of the first (266 nm) laser pulse was 330 mJ cm^{-2}. Ten ns later, the plume was intercepted by the second (213 or 266 nm) laser pulse at a fluence of 64 mJ cm^{-2}. The ICCD was gated on 5 ns from the second pulse, and remained on for 500 ns. The spectra shown were the sum of 100 events.

4. Conclusion.

In conclusion, we laser analyzed mica samples using two orthogonal laser pulses. A weak (< 330 mJ cm^{-2}) first pulse at 266 nm ablated the sample to create a material plume but no analyte emissions were observed. When the plume was intercepted transversely by a second laser pulse at 213 nm wavelength and 64 mJ cm^{-2} fluence, strong analyte emissions were induced. Without the 213 nm beam, the mLODs of the analytes were two orders of magnitude higher. The enhancement mechanism was briefly discussed. The spectral and temporal properties of the enhanced signal were consistent with our plume-LEAF model. Given the turn-key nature of the 213 nm laser and the significant signal enhancement at low mass removal, this technique should be particularly useful for minimally destructive and high spatial resolution analysis.

Acknowledgment

The research was supported by the Office of Basic Energy Sciences, Chemical Science Division of the U.S. Department of Energy under contract number DE-AC02-05CH11231 at the Lawrence Berkeley National Laboratory. The work of V.Z was supported by Laboratory Directed Research and Development (LDRD) funding from Berkeley Lab, provided by the Director, Office of Science, of the U.S. Department of Energy. The work of B.Y.C. and N.-H.C. was supported by the General Research Fund of the Research Grants Council of Hong Kong under grant number HKBU 200513 and the Faculty Research Grants of Hong Kong Baptist University.

References

[1] F.J. Fortes, J. Moros, P. Lucena, L.M. Cabalin, and J.J. Laserna, Laser-induced breakdown spectroscopy, Anal. Chem., 85 (2013) 640-669.

[2] D.W. Hahn and N. Omenetto, Laser-induced breakdown spectroscopy (LIBS), Part II: Review of instrumental and methodological approaches to material analysis and applications to different fields, Appl. Spectrosc. 66 (2012) 347-419.

[3] J. Mo, Y. Chen and R. Li, Silver jewelry microanalysis with dual-pulse laser-induced breakdown spectroscopy: 266+1064 nm wavelength combination, Appl. Opt. 53 (2014) 7516-7522.

[4] V. Zorba, X. Mao and R.E. Russo. Ultrafast laser induced breakdown spectroscopy for high spatial resolution chemical analysis, Spectrochimica Acta B, 66 (2011) 189-192.

[5] Y. Lu, V. Zorba, X. Mao, R. Zheng, and R.E. Russo, UV fs-ns double-pulse laser induced breakdown spectroscopy for high spatial resolution chemical analysis, J. Anal. At. Spectrom. 28 (2013) 743-748.

[6] P.-C. Chu, B.Y. Cai, Y.K. Tsoi, R. Yuen, K.S.Y. Leung and N.-H. Cheung, Forensic analysis of laser printed ink by X-ray fluorescence and laser-excited plume fluorescence, Anal. Chem. 85 (2013) 4311-4315.

[7] P.C. Chu, W.L. Yip, Y. Cai, and N.H. Cheung, Multi-element analysis of ceramic and polymeric samples by ArF laser excited atomic fluorescence of ablated plumes, J. Anal. At. Spectrom. 26 (2011) 1210-1216.

[8] Y. Cai, P.-C. Chu, S.K. Ho and N.-H. Cheung, Multi-element analysis by ArF laser excited atomic fluorescence of laser ablated plumes: Mechanism and applications, Front. Phys. 7 (2012) 670-678.

[9] S.K. Lau and N.H. Cheung, Minimally destructive and multi-element analysis of steel alloys by argon fluoride laser-induced plume emissions, Appl. Spectrosc. 63 (2009) 835-838.

[10] S.K. Ho and N.H. Cheung, Minimally destructive and multi-element analysis of aluminium alloys by ArF laser-induced atomic emissions, J. Anal. At. Spectrom., 22 (2007) 292-297.

[11] S.K. Ho and N.H. Cheung, Sub-part-per-billion analysis of aqueous lead colloids by ArF laser induced atomic fluorescence, Anal. Chem. 77 (2005) 193-199.

[12] Z. Wang, T.-B. Yuan, Z.-Y. Hou, W.-D. Zhou, J.-D. Lu, H.-B. Ding, and X.-Y. Zeng, Laser-induced breakdown spectroscopy in China, Front. Phys., 9, (2014) 419-438.

[13] S. K. Ho and N.H. Cheung, Sensitive elemental analysis by ArF laser-induced fluorescence of laser ablation plumes: Elucidation of the fluorescence mechanism, Appl. Phys. Lett. 87 (2005) 264104.

[14] See for example Ted Pella, Inc. website. http://www.tedpella.com/vacuum_html/Mica_Grade_V1_Properties.htm

[15] NIST Atomic Spectra Database http://www.nist.gov/pml/data/asd.cfm

[16] R.W. Coons, S.S. Harilal, S.M. Hassan, and A. Hassanein, The importance of longer wavelength reheating in dual-pulse laser-induced breakdown spectroscopy, Appl. Phys. B, 107 (2012), 873−880.

[17] R. Babar, A. Rizwan, A. Raheel, and M.A. Baig, A comparative study of single and double pulse of laser induced breakdown spectroscopy of silver, Phys. Plasmas, 18, (2011) 073301.